International Journal of Nanomedicine

Dovepress
Taylor & Francis Group

Open Access Full Text Article

ORIGINAL RESEARCH

Se-Fe Hydrogel with Switchable Hyperthermia for Osteosarcoma Therapy

Jinjie He[1,2], Jifeng Miu[1], Chao Ning[1], Shipeng Ning[3], Qingjun Wei[1,2]

[1]Department of Orthopedics, the Second Affiliated Hospital of Guangxi Medical University, Nanning, Guangxi, 530000, People's Republic of China; [2]Department of Orthopedics, the First Affiliated Hospital of Guangxi Medical University, Nanning, Guangxi, 530000, People's Republic of China; [3]Research Center of Nanomedicine Technology, the Second Affiliated Hospital of Guangxi Medical University, Nanning, 530000, People's Republic of China

Correspondence: Shipeng Ning; Qingjun Wei, Email nspdoctor@sr.gxmu.edu.cn; weiqingjun@gxmu.edu.cn

Introduction: Clinical treatment of osteosarcoma remains challenging because of residual tumor–associated recurrence, bacterial infection, and insufficient bone reconstruction. To address these challenges, a selenium–iron Prussian blue nanocube (FeSePB) was designed and encapsulated within a thermoresponsive hydrogel for osteosarcoma therapy.

Methods: The FeSePB nanocube functions as an efficient photothermal conversion agent, producing localized heating under near-infrared (NIR) irradiation and enabling controlled softening of the hydrogel after implantation under laser irradiation. Following administration into the osteosarcoma site, initial NIR irradiation triggered hydrogel softening and rapid release of FeSePB, resulting in elevated local temperature that eliminated residual tumor cells and achieved antibacterial effects through photothermal therapy (PTT). Concurrent selenium release further inhibited bacterial growth, reducing infection risk.

Results: In vitro experiments demonstrated that sustained mild PTT induced moderate hyperthermia, which supported bone regeneration. In vivo animal experiments demonstrated remarkable tumor growth inhibition, with inhibition rates of about 90.67% compared with the control group. Thus, the FeSePB hydrogel demonstrated NIR-switchable temporal regulation, enabling integrated anti-tumor, anti-infective, and pro-osteogenic functions during osteosarcoma treatment.

Conclusion: This strategy offers a multifunctional therapeutic platform that simultaneously addresses tumor proliferation, infection, and bone loss, highlighting its potential for clinical translation.

Keywords: osteosarcoma, thermal-responsive hydrogel, PTT, antibacterial, bone reconstruction

Introduction

Bone tumors significantly compromise patient health and are broadly classified as benign or malignant, each showing different biological behaviors and therapeutic responses.[1] Osteosarcoma is the most prevalent malignant primary bone tumor and is defined by the production of immature bone or osteoid by malignant cells. Its incidence shows a bimodal age distribution, with a peak during adolescence, coinciding with rapid skeletal growth, and a second peak in adults aged 60 years or older.[2] Osteosarcoma can occur in any bone, but it most frequently involves the regions around the knee and the proximal humerus.[3] Current treatment strategies mainly rely on surgical resection of the primary tumor and surrounding tissues, combined with chemotherapy or other adjuvant approaches.[4] Although low-grade osteosarcomas are generally managed effectively by surgery alone, outcomes for high-grade tumors remain unsatisfactory. These aggressive tumors carry a high risk of metastasis to the lungs, lymph nodes, and other organs, and therapeutic advances have been limited since the establishment of the neoadjuvant chemotherapy–surgery–adjuvant chemotherapy regimen in the 1980s.[5,6] During surgical intervention, careful consideration of resection margins is required to achieve complete tumor removal while minimizing excessive bone loss. Thus, there is an urgent need to develop new therapeutic strategies that can simultaneously eradicate osteosarcoma cells and support bone repair to achieve optimal therapeutic outcomes.

Three major challenges continue to hinder effective osteosarcoma treatment: tumor recurrence, bacterial infection, and impaired bone regeneration.[7,8] Persistent inflammation triggered by bacterial infection, together with the release of inflammatory mediators, creates an immunosuppressive and pro-angiogenic microenvironment.[9,10] Such conditions

https://doi.org/10.2147/IJN.S594220
Received: 22 January 2026
Accepted: 22 May 2026
Published: 23 June 2026

promote the survival, proliferation, and metastasis of residual tumor cells, increasing the risk of recurrence.[11] In this context, photothermal therapy (PTT) has gained increasing interest as an emerging approach for tumor ablation and antibacterial treatment.[12] Photothermal conversion agents absorb incident light energy, leading to excitation of internal electrons and rapid conversion of this energy into heat upon relaxation.[13–16] This process occurs within a very short time frame and results in a sharp increase in local temperature. For effective tumor cell killing and antibacterial activity, temperatures at the lesion site typically need to exceed 50 °C. However, exposure to such high temperatures risks collateral damage to surrounding healthy tissues due to heat diffusion. To address this limitation, mild hyperthermia in the range of 40–44 °C has been proposed as an alternative, as it can induce tumor cell death and exert antibacterial effects while causing less damage to normal tissues, making it more suitable for clinical application.[17]

A variety of nano-photothermal conversion agents have been developed to achieve mild PTT, and these materials can be broadly categorized into organic small molecules and inorganic nanomaterials.[18–20] Representative platforms include carbon-based nanostructures, noble metal nanomaterials, and layered black phosphorus.[21–24] For example, Wang et al reported an organic nanoparticle capable of inducing mild hyperthermia under 650 nm laser irradiation, resulting in efficient *Escherichia coli* clearance and alleviation of inflammation.[25] Lin et al developed a single-atom palladium nanozyme that promoted ferroptosis-enhanced mild PTT, improving anti-tumor efficacy while minimizing damage to normal tissues.[26] More recently, gold nanoaggregates with a high photothermal conversion efficiency of 92.8% were synthesized and achieved complete tumor ablation.[27] Despite these promising advances in both tumor elimination and antibacterial therapy, efficient and precise delivery of nano-photothermal agents to target sites remains a major challenge. Many of these nanomaterials lack intrinsic tumor-targeting properties and exhibit low bioavailability, limiting their therapeutic performance and clinical translation.

Besides tumor recurrence and bacterial infection, impaired bone regeneration represents another critical challenge in osteosarcoma treatment.[28] The skeletal system plays an essential role in structural support and organ protection and is composed of more than 60% inorganic components.[29] Although bone tissue has an intrinsic capacity for regeneration following limited injury, bone loss caused by tumor invasion or surgical resection frequently exceeds the threshold for self-repair.[30] Therefore, a variety of nanomaterial-based strategies have been developed to promote bone regeneration.[31,32] It is worth noting that the extracellular matrix (ECM) of bone plays a key role in promoting osteogenesis.[33,34] Injectable hydrogels incorporating organic molecules or nanomaterials and mimicking the viscoelastic properties of the ECM have been considered promising candidates for bone repair.[35] These hydrogels facilitate bone cell proliferation and tissue regeneration while offering advantages such as minimal invasiveness and close tissue adhesion.[24] However, most existing hydrogel systems primarily focus on bone regeneration and overlook the need to clear residual osteosarcoma and meet antibacterial requirements.

Persistent inflammatory responses triggered by bacterial infection create an immunosuppressive microenvironment that favors the proliferation and metastasis of residual tumor cells, increasing the risk of tumor recurrence.[36–38] Furthermore, the hyperinflammatory tumor microenvironment continuously suppresses osteogenic differentiation, severely limiting bone regeneration.[30,33] Structural instability and tissue necrosis at bone defect sites further promote bacterial biofilm formation on implants or necrotic bone surfaces, exacerbating the persistence of infection and difficulty of treatment.[20,34] This complex, interconnected pathological cascade renders traditional staged or single-target therapies insufficient for effectively addressing these complications in a coordinated manner.[24] Therefore, nanomaterials designed for osteosarcoma treatment must integrate synergistic anti-tumor, antibacterial, and pro-bone regenerative functions.

Selenium (Se) played a crucial role in various biological functions. Considering that the rational complex of Se and other metal could significantly improve the physicochemical properties,[39] a FeSePB nanocube was incorporated into a low-temperature agarose hydrogel for osteosarcoma therapy in this work (Scheme 1). Agarose was selected for its shear-thinning injectability, excellent biocompatibility, FDA-recognized status, and thermally reversible gelation that enables mild drug loading and NIR-triggered synergistic therapy with FeSePB. Following in situ injection into the target area, treatment was initiated using 808 nm laser irradiation. The FeSePB-loaded hydrogel acted as a photothermal conversion agent, converting light energy into heat and generating mild hyperthermia at the local site, reaching 45.2 °C. This temperature was sufficient to suppress tumor cell activity while eliminating bacteria. Simultaneously, hydrogel softening enabled sustained selenium release, providing continuous antibacterial effects. During bone regeneration, near-

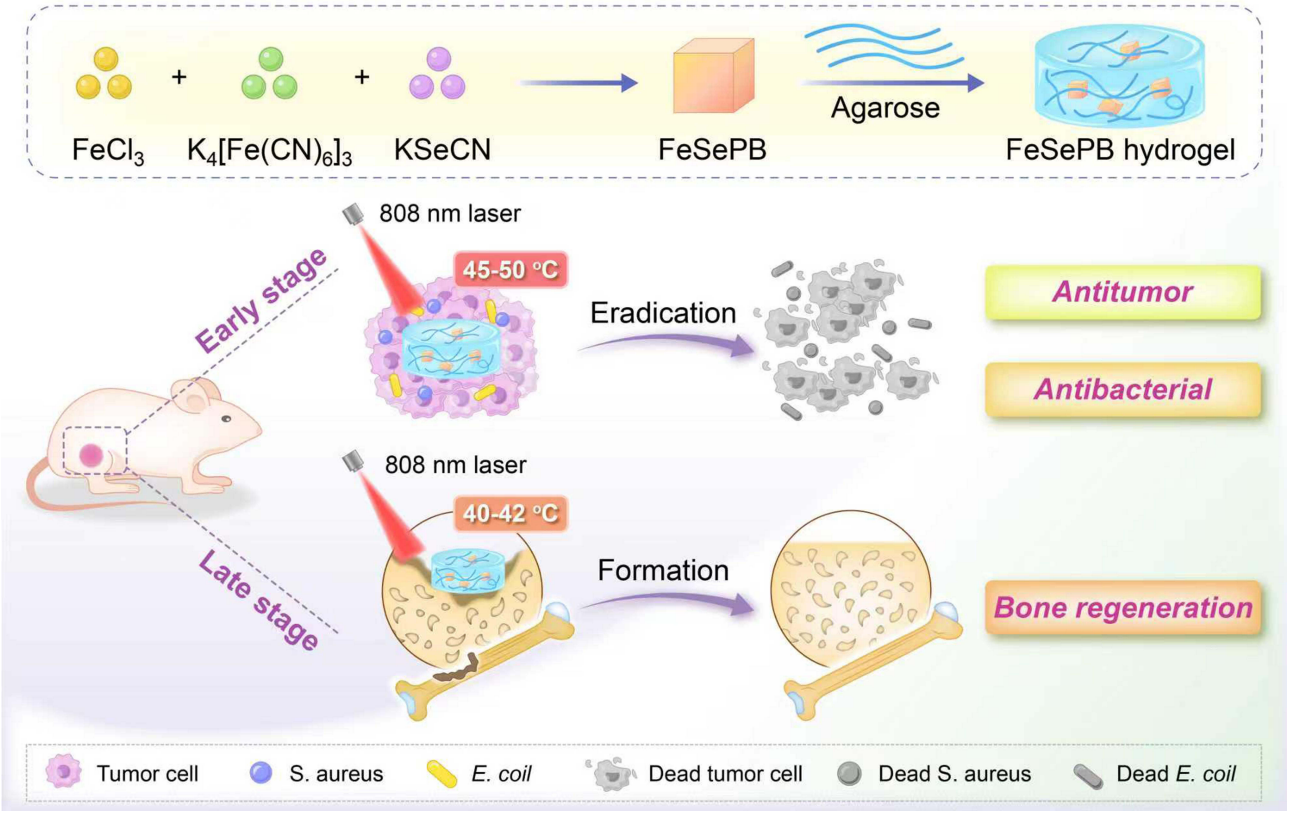

Scheme 1 Schematic illustration of the "three-in-one" hydrogel enabling tumor ablation, antibacterial therapy, and promotion of bone regeneration under mild PTT.

infrared laser–triggered mild hyperthermia promoted osteogenic activity, while the softened FeSePB hydrogel formed a porous three-dimensional scaffold conducive to bone tissue ingrowth. This strategy disrupts the pathological cycle of tumor recurrence, bacterial infection, and impaired bone repair, achieving synergistic therapeutic efficacy through PTT.

Result and Discussion

Characterization of FeSePB Nanoparticles and Hydrogel

$K_4(Fe(CN)_{63}$ and $FeCl_3$ was employed as the precursor, with potassium selenocyanate (KSeCN) introduced as the dopant during the synthesis process, thus yielding selenium-doped Prussian blue (FePB), denoted as FeSePB. Full synthetic protocols are available in the Supplementary material. The transmission electron microscopy (TEM) characterization results of FeSePB are presented in Figure 1A, which demonstrates that FeSePB exhibits a square morphology analogous to that of pristine Prussian blue. Subsequently, FeSePB was dispersed in an agarose hydrogel matrix to enhance its injectability and long-term stability. The scanning electron microscopy (SEM) image of the resulting hydrogel is displayed in Figure 1B, revealing a sophisticated three-dimensional porous network architecture. Furthermore, the particle size of FeSePB was determined via dynamic light scattering (DLS) measurements, as illustrated in Figure 1C. The average particle sizes of FeSePB batches synthesized repetitively over three consecutive days were measured to be 96.8 ± 5.4 nm, 108.2 ± 8.5 nm and 103.3 ± 7.8 nm, respectively, indicating a homogeneous particle size distribution of FeSePB. In addition, Figure S1 depicts the variations in the particle size of FeSePB suspended in phosphate-buffered saline (PBS) and RPMI-1640 medium. The results further confirm that FeSePB possesses robust stability without observable degradation, rendering it a promising candidate for subsequent biological experiments. The high-resolution X-ray photoelectron spectroscopy (XPS) spectra of FeSePB, presented in Figure 1D and E, exhibit the characteristic peaks corresponding to the Fe 2p and Se 3d orbitals, respectively.

https://doi.org/10.2147/IJN.S594220

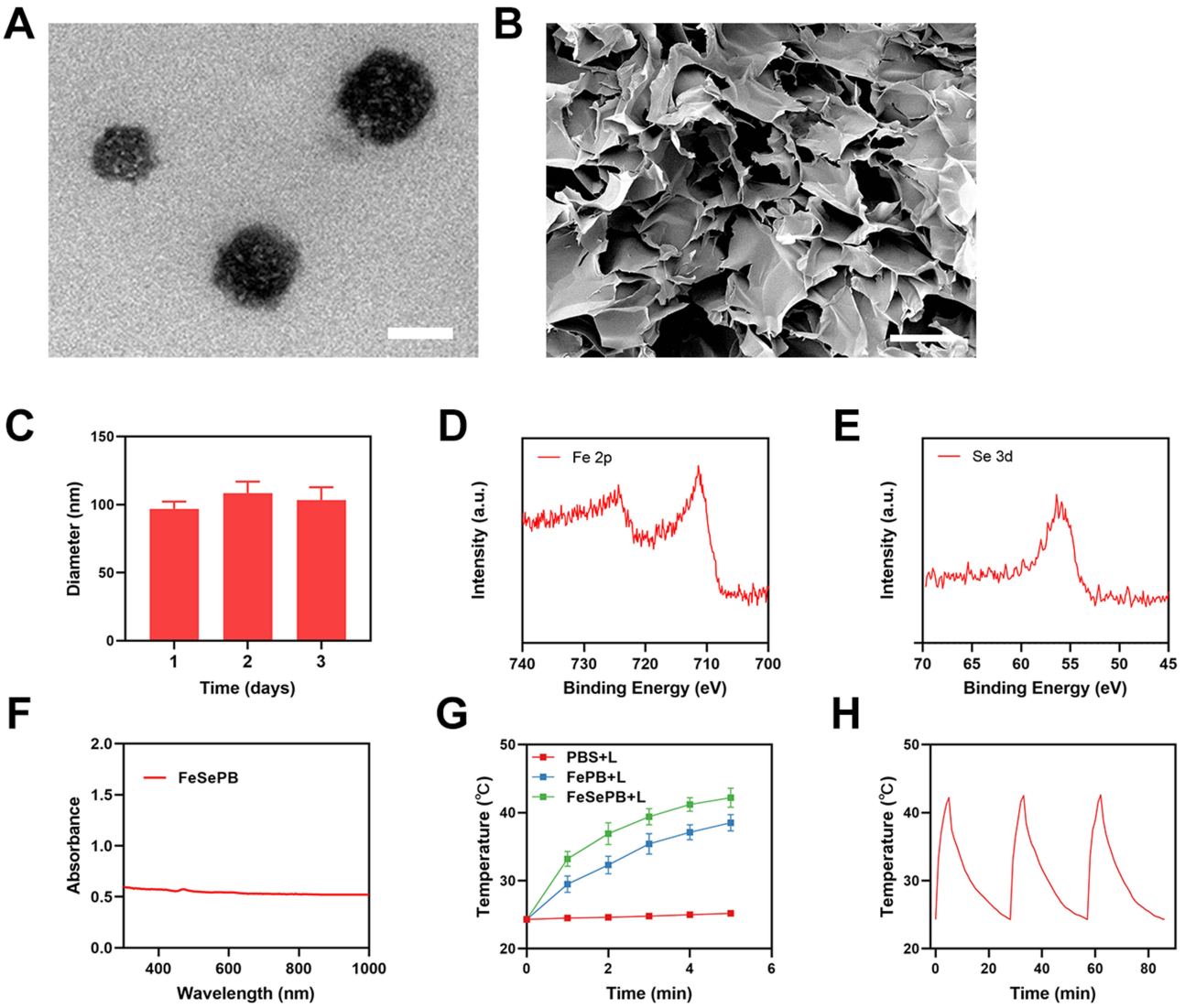

Figure 1 (**A**) TEM image of FeSePB. Scale bar: 100 nm. (**B**) SEM image of FeSePB-based hydrogel. Scale bar: 20 μm. (**C**) Particle size of FeSePB revealed by DLS detection. (**D**) Fe 2p high-resolution XPS spectra of FeSePB. (**E**) Se 3d high-resolution XPS spectra of FeSePB. (**F**) UV-vis absorption spectra of FeSePB. (**G**) Temperature rise curves of different groups under 808 nm laser irradiation. Laser: (L) (**H**) Temperature variation curves of FeSePB after three consecutive laser irradiations.

Photothermal Property Evaluation

For a material to serve as an efficient photothermal agent, it is essential to possess strong absorption in the near-infrared (NIR) region. As illustrated in Figure 1F, the UV-vis absorption spectrum of FeSePB was investigated, and the results demonstrate that FeSePB features a broad absorption band across a wide wavelength range including 808 nm, which highlights its great potential as a high-performance photothermal agent. PBS was used as the control group, FeSePB and FePB samples were irradiated continuously with an 808 nm laser, and the real-time temperature changes were recorded using a thermal infrared camera. As shown in Figure 1G, the temperature of the PBS group increased by less than 2 °C within 5 minutes, while the temperature rise of the FePB group reached approximately 14.2 °C. Notably, FeSePB exhibited the most prominent photothermal effect, with its temperature increasing from 24.3 °C to 42.2 °C. Furthermore, to verify the photothermal stability of FeSePB, three consecutive cycles of 808 nm laser irradiation were conducted (Figure 1H). The results confirmed that FeSePB maintained excellent stability during the three heating-cooling cycles, without significant attenuation of its photothermal performance. In addition, to evaluate whether the agarose hydrogel would affect the photothermal response capability of FeSePB, a comparative study on the temperature rise behavior was performed between the FeSePB-loaded hydrogel (with the same FeSePB concentration) and the pure FeSePB solution.

The temperature elevation effects of the two systems were found to be quite close, indicating that the agarose hydrogel had negligible influence on the photothermal curve of FeSePB (Figure S2). We have explored the injectability of the FeSePB-loaded agarose hydrogel at room temperature, as shown in Figure S3, this FeSePB hydrogel could be injected at room temperature. Moreover, the temperature-responsive rheological curves of the FeSePB hydrogel confirmed the sustained-release capability of the hydrogel matrix, as evidenced by the gradual decrease in its storage modulus with increasing temperature (Figures S4 and S5). Collectively, the agarose hydrogel serves as an ideal carrier that maintains the photothermal performance of FeSePB while providing sustained-release functionality, laying a solid foundation for its subsequent biological applications.

In vitro Antitumor Study

Given the favorable material characterization results, we further investigated the efficacy of FeSePB hydrogel combined with an 808 nm laser for antibacterial and antitumor applications, with the antitumor capacity evaluated first. Controllable drug release from photothermal hydrogels is of great significance to their biological functions and therapeutic efficacy. As shown in Figure S6, with laser irradiation, the materials are gradually released, and after turning off the laser, the hydrogel slowly solidifies. As presented in Figures 2A and S7, fluorescein diacetate (FDA) and propidium iodide (PI) double staining were employed to assess cell viability under different treatment conditions. FDA emits green fluorescence, serving as a marker for viable cells. In contrast, when cells undergo apoptosis, the damaged cell membrane allows PI to penetrate and intercalate into DNA, resulting in red fluorescence. Notably, no apoptotic signals were detected in cells treated with the laser alone or FePB alone, indicating that neither single laser irradiation nor standalone FePB could induce hyperthermia or other substantial cellular damage. FeSePB hydrogel alone exhibited a certain degree of cytotoxicity, which was attributed to the reactive oxygen species (ROS) generated by the sustained release of FeSePB from the hydrogel matrix, enabling direct tumor cell killing. FePB hydrogel combined with laser (FePB + L) induced extensive cellular apoptosis, yet a fraction of cells remained viable. Of great significance, FeSePB hydrogel combined with laser (FeSePB + L) achieved the most potent apoptotic effect, with almost no green fluorescent signals observed, demonstrating its superior tumor-killing capacity. The ROS generation in each group was detected using 2′,7′-dichlorodihydrofluorescein diacetate (DCFH-DA) (Figure 2B), and the results were consistent with the live/dead cell staining data. The FeSePB + L group not only exerted the strongest cytotoxicity but also induced the brightest green fluorescence corresponding to ROS accumulation. Quantitative analysis of the fluorescence intensity further revealed a statistically significant difference between the FeSePB + L group and the FePB + L group (Figure 2D). The capacity of FeSePB + L to inhibit tumor cell proliferation was further evaluated using a commercial CCK-8 assay kit, with treatments administered after the incubation period. As shown in Figure 2C, the cell viability in the FePB + L group was approximately 53.12%, whereas that in the FeSePB + L group drastically decreased to around 18.44%. Additionally, the tumor-killing efficacy of FeSePB combined with laser at different concentrations was investigated, and the results (Figure 2E) demonstrated a concentration-dependent enhancement in the antitumor activity of FeSePB. These findings collectively reveal that Se doping endows FeSePB with synergistic photothermal-ROS therapeutic effects that surpass those of pristine FePB, and the agarose hydrogel carrier optimizes its bioavailability.

Evaluation of Bone Repair Performance

In the tumor microenvironment, abnormally accumulated inflammatory factors establish a persistent hyperinflammatory homeostasis. This homeostatic state not only blocks the osteogenic pathway by downregulating osteogenesis-related transcription factors and inhibiting the proliferation and differentiation of osteoblasts but also activates the excessive activation program of osteoclasts, disrupting the dynamic balance between bone resorption and bone formation. Hence, we further investigated the bone repair efficacy of FeSePB. As shown in Figure 3A, the live/dead cell staining results of bone marrow mesenchymal stem cells (BMSCs) co-incubated with different treatment groups demonstrated that the FeSePB + L group exerted no cytotoxic effects on BMSCs. Additionally, the cell viability was analyzed after 24 h and 48 h of incubation, and the results (Figure 3B) indicated that the FeSePB + L group significantly enhanced the viability of BMSCs compared with other groups. To further explore the osteogenic differentiation-promoting effect, key indicators involved in osteogenic differentiation were evaluated, including Runx2 (the master transcription factor for osteogenic differentiation), ALP (the early functional marker of osteogenic differentiation), Col-I (the main structural protein

 https://doi.org/10.2147/IJN.S594220

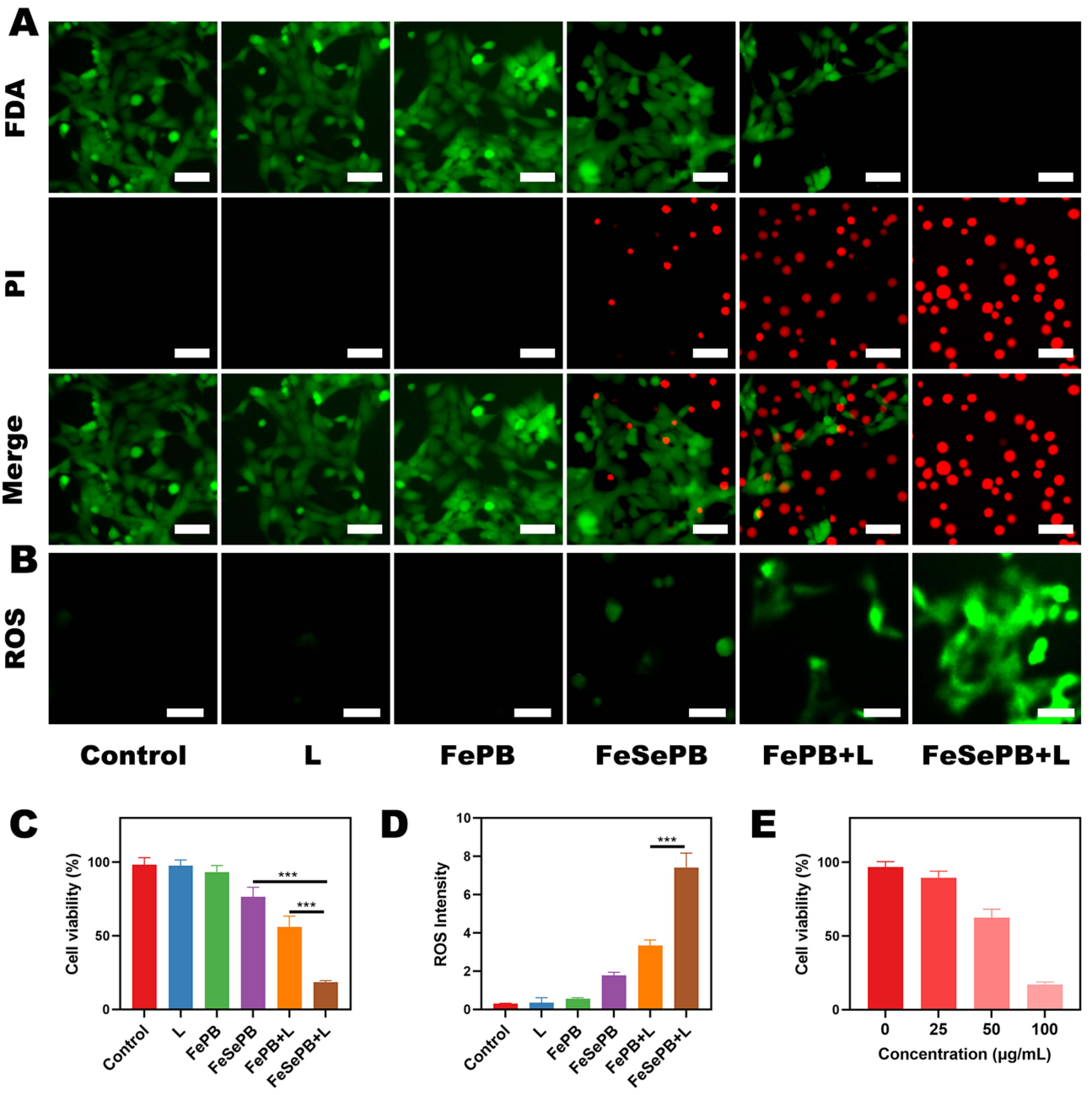

Figure 2 (**A**) Fluorescence images of the K7M2 cells after the different treatments. Live cells are shown in green and dead cells are shown in red, Scale bar: 20 μm. (**B**) Measurement of tumor cell ROS fluorescence after the different treatments. Scale bar: 20 μm. (**C**) Cell viability after indicated treatment. (**D**) Quantitative analysis of ROS production after the different treatments. (**E**) Cell viability after treatment with different concentrations of FeSePB hydrogel under laser irradiation. (N=3) *** $p < 0.005$; Student's *t*-test.

composing the bone matrix), and OCN (the late mineralization marker of osteogenic differentiation). After FeSePB treatment combined with laser irradiation, all the above indicators (Figure 3B–E) showed a certain degree of upregulation after one week of culture, suggesting that the mild hyperthermia induced by FeSePB and laser treatment could promote the early osteogenic differentiation of BMSCs. Notably, as an indicator involved in the initial stage of extracellular matrix mineralization, the ALP activity was detected after 3 and 7 days of incubation, respectively. The results also revealed that the FeSePB + L group significantly improved the functional maturation of osteoblasts. The osteogenic differentiation process is accompanied by distinct changes in cell morphology, when undergoing directed differentiation into osteoblasts, the cells gradually spread into polygonal or cobblestone-like shapes, and F-actin assembles into

https://doi.org/10.2147/IJN.S594220

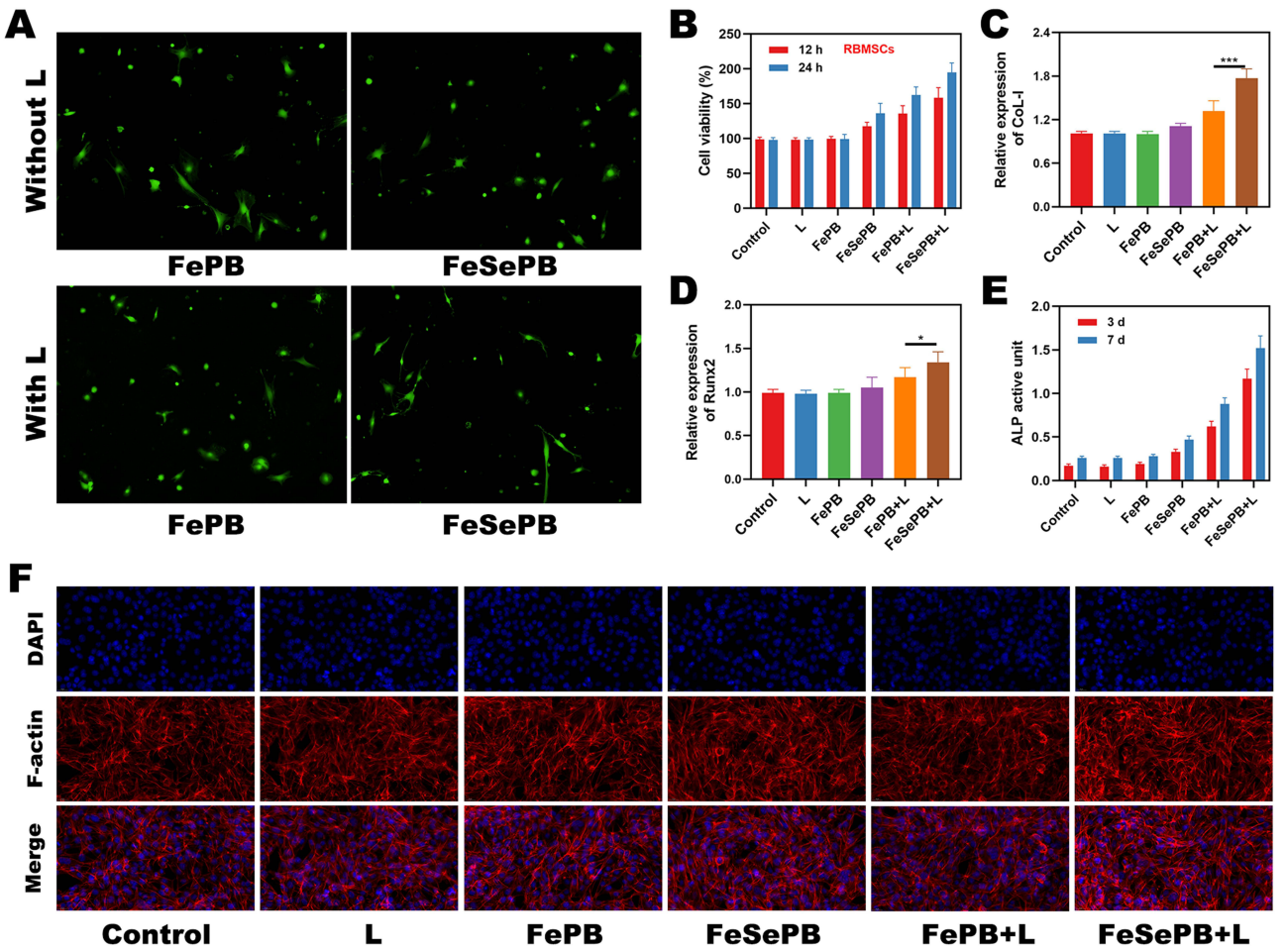

Figure 3 (**A**) Live/dead staining images of BMSCs under various treatments. (**B**) Cell viability at different time periods after indicated treatment. (**C–E**) CoL-1, Runnx2 and ALP activity. (**F**) CLSM images of F-actin immunofluorescence under different treatments. (N=3) * p <0.05, *** p < 0.005; Student's *t*-test.

parallelly arranged stress fibers, forming a clear cytoskeletal network that anchors cell polarity and supports the secretion of extracellular matrix and the formation of mineralized nodules. As presented in Figure 3F, the cells treated with the FeSePB + L group had entered the osteogenic differentiation state. These results confirmed that FeSePB, under laser irradiation, not only exhibits excellent biocompatibility with BMSCs but also promotes their proliferation and directional differentiation into osteoblasts through mild photothermal effects.

Photoactivated Antibacterial Efficacy

Persistent inflammatory microenvironment induced by bacterial infection can reshape the local tumor immune landscape and establish an immunosuppressive barrier, thereby providing a favorable niche for the proliferation and invasion of dormant tumor cells. This process significantly impairs the efficiency of anti-tumor immune responses in the host and further elevates the potential risk of tumor recurrence and distant metastasis. Consequently, we evaluated the photo-activated antibacterial efficacy mediated by FeSePB. Experiments were performed using *Staphylococcus aureus* (S. aureus) and *Escherichia coli* (E. coli). As illustrated in Figure 4A, S. aureus proliferated normally in the PBS group and the L alone group, exhibiting dense colony distribution on the agar plates. In contrast, the FeSePB-treated group without laser irradiation showed a moderate inhibitory effect on S. aureus growth. Notably, after synergistic laser irradiation, the FeSePB-treated group displayed sparsely distributed S. aureus colonies on the plates. Similarly, the growth of E. coli was completely abrogated in the FeSePB + L group, which further confirmed the superior antibacterial efficacy triggered by photoactivated FeSePB. Furthermore, semi-quantitative analysis of the bacterial survival index on

https://doi.org/10.2147/IJN.S594220

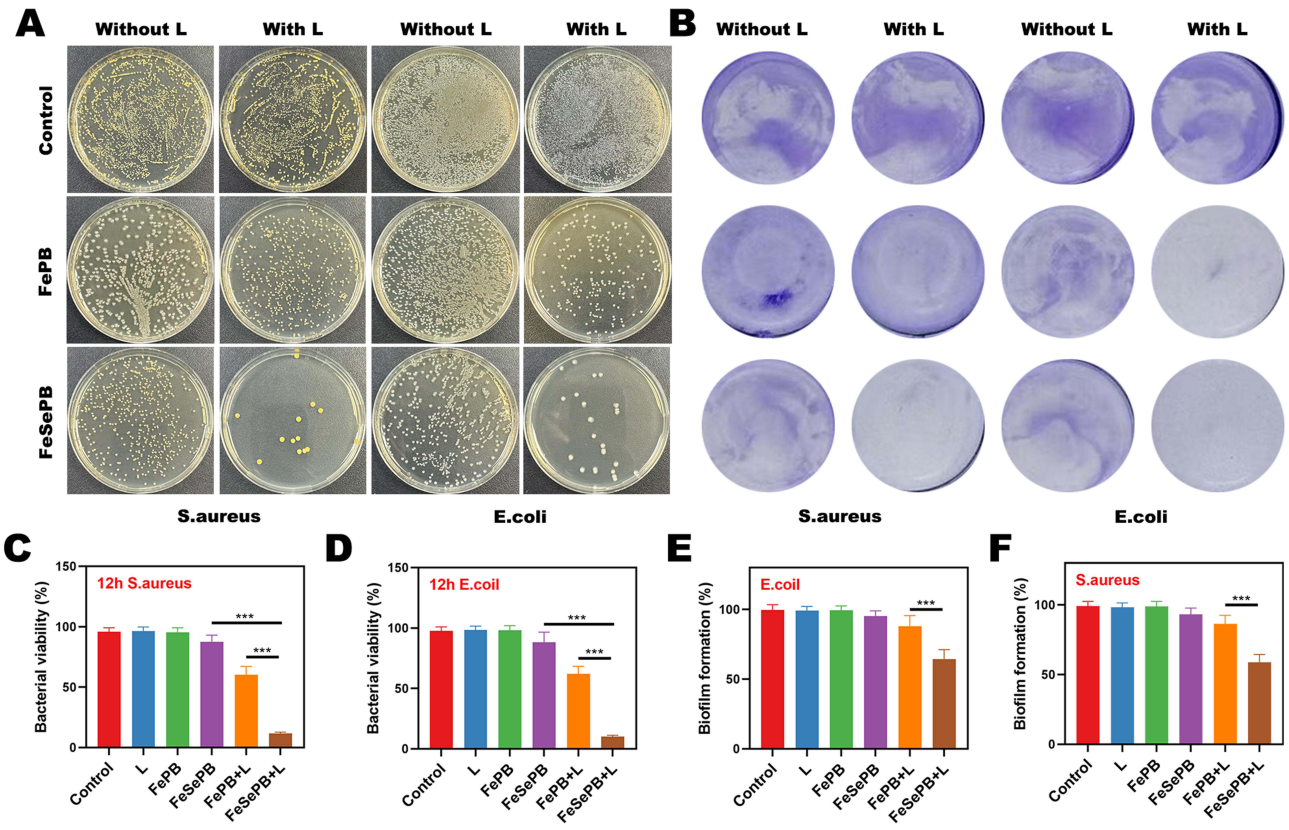

Figure 4 (**A**) Optical photographs of the viability rate of S. aureus and E. coil grown on agar plates with different treatments. (**B**) Biofilm crystal violet staining images of bacteria with different treatments. (**C** and **D**) Semi-quantitative analysis of the viability rate in (**A**). (**E** and **F**) Semi-quantitative analysis of the viability rate in (**B**). (N=3) *** $p < 0.005$; Student's *t*-test.

the plates was conducted, and the results are presented in Figures 4C and D. The survival fractions of E. coli and S. aureus in the FeSePB + L group were approximately 10.12 ± 1.42% and 11.8 ± 1.17%, respectively, which were significantly different from those in the FePB + L group (55.41 ± 4.59% and 60.42 ± 4.76%, respectively). Bacteria tend to adhere and proliferate to form biofilms; therefore, we further investigated the inhibitory capacity of FeSePB + L on biofilm formation of the two bacterial strains, with crystal violet staining for analytical purposes. As shown in Figure 4B, distinct biofilm coatings were observed in the PBS, L alone, and FePB groups. In contrast, the FeSePB group showed relatively faint crystal violet staining, and the FeSePB + L group exhibited almost no overlapping bacterial colonies. Quantitative results further verified that the FeSePB + L group suppressed the formation rate of bacterial biofilms (Figure 4E and F), indicating that FeSePB combined with photothermal effects can disrupt the structural integrity of biofilms to effectively inhibit bacterial proliferation.

In vivo Anti-Tumor Study

Given the favorable in vitro antibacterial, antitumor, and osteogenesis-promoting capacities of FeSePB combined with L irradiation, we further investigated FeSePB-based in vivo antitumor efficacy. First, we verified the temperature elevation effect of FeSePB hydrogel in mouse tumors in response to L irradiation. As shown in Figure 5A, the PBS group exhibited almost no temperature increase, while both FePB and FeSePB groups showed a temperature elevation effect, with FeSePB inducing a more pronounced temperature rise. Further temperature rise curves recorded by an infrared thermal camera revealed that the tumors of mice in the FeSePB group increased in temperature by approximately 13.8°C under continuous L irradiation for 5 minutes (Figure 5B). Tumor cells are less thermotolerant than normal cells. Typically, their viability decreases at 42–46°C, enabling hyperthermic ablation of tumors. We then established a mouse subcutaneous tumor model, which was divided into

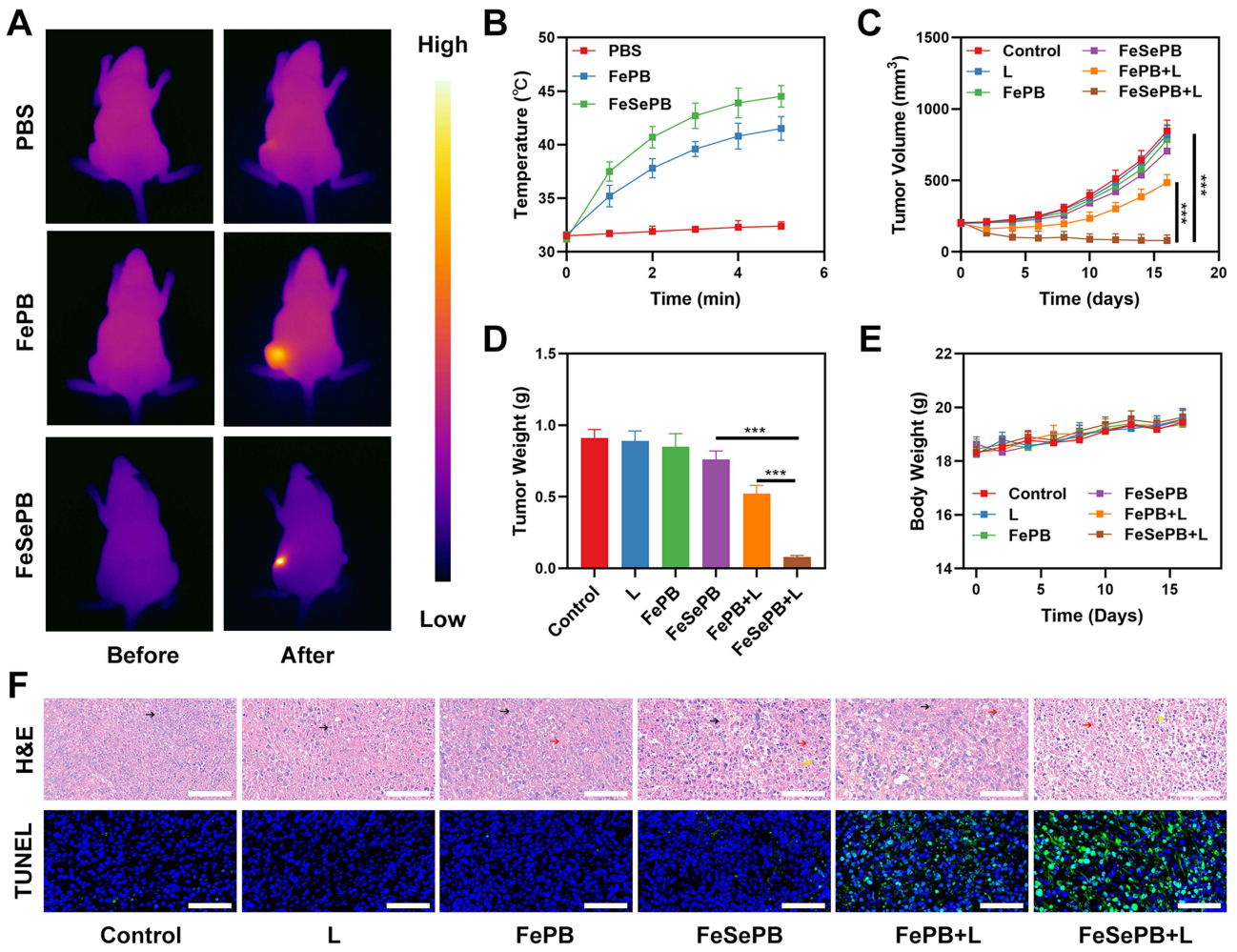

Figure 5 (**A** and **B**) Temperature increases in mice implanted with K7M2 tumors following 808 nm laser irradiation (1 W/cm^2) for 5 min in the indicated treatment. (**C**) Tumor volume change over time in groups treated as indicated. (**D**) Average tumor weight values associated with the indicated treatments. (**E**) Body weight curves following the indicated treatments in mice. (**F**) Representative H&E and TUNEL-stained tumor sections from mice in the indicated treatment groups. Black arrow: normal tumor cells. Red arrow: homogeneously eosinophilic structure. Scale bars: 100 μm. (N=3) *** $p < 0.005$; Student's *t*-test.

the following groups: (1) Control, (2) L, (3) FePB, (4) FeSePB, (5) FePB + L and (6) FeSePB + L.Tumor volumes in the control group proliferated rapidly, increasing from approximately 200 mm^3 to about 840 mm^3 within 16 days (Figure 5C), and the proliferation trend in the L alone group was similar to that in the control group, indicating that laser stimulation alone had no antitumor effect. The FeSePB group showed a slight inhibition of tumor volume, while the FePB + L group exhibited a moderate inhibition of tumor volume, which was attributed to the ability of FePB to mediate a certain degree of PTT in response to L irradiation. In contrast, tumor growth in the FeSePB + L group was completely inhibited without any proliferation trend during the treatment cycle. This observation suggested that light-controlled FeSePB release not only generates hyperthermia to kill tumor cells but also enables FeSePB to catalyze the production of ROS for further tumor tissue destruction; the synergy of these two effects achieves maximized antitumor efficacy. After the treatment, mouse tumors were excised and weighed, and the results were consistent with the trend of tumor volume growth, confirming that the FeSePB + L group achieved the optimal therapeutic effect compared with other experimental groups (Figure 5D). In addition, as shown in Figure 5E, the body weights of mice in all groups increased steadily during the treatment period without sudden death, verifying the favorable biosafety of the designed hydrogel delivery system. Furthermore, tumor tissues from mice were collected for sectioning, followed by tissue immunofluorescence staining and pathological analysis. The results are shown in Figure 5F, the FePB + L group exhibited a certain therapeutic effect, while

https://doi.org/10.2147/IJN.S594220

notably, the FeSePB + L group showed extensive tumor cell necrosis and distinct TUNEL-positive apoptotic signals. Moreover, pathological results of sections of major mouse organs (heart, liver, spleen, lung, and kidney) demonstrated no abnormal signals or inflammatory response indicators in the FeSePB + L group, further highlighting the safety of this therapeutic strategy (Figure S8). Further investigation on blood biochemical analysis proved biosafety of FeSePB+L (Figure S9). All in all, these in vivo findings confirm that FeSePB hydrogel combined with L irradiation exerts potent and safe antitumor effects by synergizing photothermal therapy and ROS-mediated cytotoxicity.

Conclusion

In summary, we constructed a FeSePB-based photoresponsive hydrogel system that integrates three synergistic functional modules: antitumor, anti-infection, and osteogenesis promotion. In vitro experiments confirmed that FeSePB combined with L irradiation can convert light energy into thermal energy, which not only induces hydrogel softening and sustained release of selenium elements but also achieves efficient killing of two typical pathogenic bacteria (*S. aureus* and *E. coli*) while promoting osteogenic regeneration. In vivo experiments further verified that FeSePB synergized with L irradiation generates mild hyperthermia in local tissues, thereby exerting robust subsequent antitumor efficacy. The multifunctional platform developed in this study could interrupt the vicious cycle among tumor proliferation, bacterial infection, and impaired bone regeneration. Further investigations will be performed in future research to evaluate its translational potential.

Acknowledgments

This work is supported by the Open Project of Guangxi Key Laboratory of Regenerative Medicine, Guangxi Medical University (grant number: Guizaichongkai202301), the Self-funded Research Project Administration of Traditional Chinese Medicine of Guangxi Zhuang Autonomous Region (grant number: GXZYA20230301) and the Self-funded scientific research project of the Health Commission of Guangxi Zhuang Autonomous Region (grant number: Z-A20250545). Animal experiments in this work met the criteria of the Ethical Review Committee. All animal procedures were approved by the Medical Ethics Committee of the Second Affiliated Hospital of Guangxi Medical University (Approval No. 2025-KYL(068)) and were conducted in accordance with the Guidelines for the Ethical Review of Laboratory Animal Welfare (GB/T 35892-2018, China).

Disclosure

The authors report no conflicts of interest in this work.

References

1. Cole S, Gianferante DM, Zhu B, Mirabello L. Osteosarcoma: a surveillance, epidemiology, and end results program-based analysis from 1975 to 2017. *Cancer*. 2022;128(11):2107–2118. doi:10.1002/cncr.34163
2. Beird HC, Bielack SS, Flanagan AM, et al. Osteosarcoma. *Nat Rev Dis Prim*. 2022;8(1):77. doi:10.1038/s41572-022-00409-y
3. Tian H, Cao J, Li B, et al. Managing the immune microenvironment of osteosarcoma: the outlook for osteosarcoma treatment. *Bone Res*. 2023;11(1):11. doi:10.1038/s41413-023-00246-z
4. Tal A, Gunawardana-Zeigler S, Peng D, et al. Inhibition of DKK-1 by WAY262611 inhibits osteosarcoma metastasis. *Mol Cancer Ther*. 2025;24(5):728–739. doi:10.1158/1535-7163.MCT-24-0744
5. Yu S, Yao X. Advances on immunotherapy for osteosarcoma. *Mol Cancer*. 2024;23(1):192. doi:10.1186/s12943-024-02105-9
6. Gill J, Gorlick R. Advancing therapy for osteosarcoma. *Nat Rev Clin Oncol*. 2021;18(10):609–624. doi:10.1038/s41571-021-00519-8
7. Kortam S, Lu Z, Zreiqat H. Recent advances in drug delivery systems for osteosarcoma therapy and bone regeneration. *Commun Mater*. 2024;5(1):168. doi:10.1038/s43246-024-00612-2
8. Wang L, Huang Y, Zhang X, Chen W, Dai Z. Exosomes derived from FN14-overexpressing BMSCs activate the NF-κB signaling pathway to induce PANoptosis in osteosarcoma. *Apoptosis*. 2025;30(3):880–893. doi:10.1007/s10495-024-02071-z
9. Geng C, He S, Yu S, et al. Achieving clearance of drug-resistant bacterial infection and rapid cutaneous wound regeneration using an ROS-balancing-engineered heterojunction. *Adv Mater*. 2024;36(16):2310599. doi:10.1002/adma.202310599
10. Puthia M, Petrlova J, Petruk G, et al. Bioactive suture with added innate defense functionality for the reduction of bacterial infection and inflammation. *Adv Funct Mater*. 2023;12(31):2300987. doi:10.1002/adhm.202300987
11. Li W, Wu J, Zhang J, et al. Puerarin-loaded PEG-PE micelles with enhanced anti-apoptotic effect and better pharmacokinetic profile. *Drug Deliv*. 2018;25(1):827–837. doi:10.1080/10717544.2018.1455763

12. Wang Y, Xu Y, Song J, et al. Tumor cell-targeting and tumor microenvironment-responsive nanoplatforms for the multimodal imaging-guided photodynamic/photothermal/chemodynamic treatment of cervical cancer. *Int J Nanomed*. 2024;19:5837–5858. doi:10.2147/IJN.S466042
13. Wu M, Xiao Y, Wu R, Lei J, Li T, Zheng Y. Aggregable gold nanoparticles for cancer photothermal therapy. *J Mater Chem B*. 2024;12 (33):8048–8061. doi:10.1039/D4TB00403E
14. Yang R, Yu X, Wei C, Wu C, Zhang W. Fe3O4 clusters with high photothermal performance for photothermal therapy of tumor. *Chem Eng J*. 2025;504:159045. doi:10.1016/j.cej.2024.159045
15. Qi P, Zhang J, Bao Z, Liao Y, Liu Z, Wang J. A platelet-mimicking single-atom nanozyme for mitochondrial damage-mediated mild-temperature photothermal therapy. *ACS Appl Mater Interfaces*. 2022;14(17):19081–19090. doi:10.1021/acsami.1c22346
16. Ma Z, Foda MF, Liang H, Zhao Y, Han H. In situ nanozyme-amplified nir-ii phototheranostics for tumor-specific imaging and therapy. *Adv Funct Mater*. 2021;31(37):2103765. doi:10.1002/adfm.202103765
17. Tao N, Jiao L, Li H, et al. A mild hyperthermia hollow carbon nanozyme as pyroptosis inducer for boosted antitumor immunity. *ACS Nano*. 2023;17(22):22844–22858. doi:10.1021/acsnano.3c07601
18. Chen W, He C, Qiao N, et al. Dual drugs decorated bacteria irradiate deep hypoxic tumor and arouse strong immune responses. *Biomaterials*. 2022;286:121582. doi:10.1016/j.biomaterials.2022.121582
19. Hu X, Ma R, Zhang P, et al. Biomimetic metal–organic framework combats biofilm-associated infections via hyperthermia-enhanced bacterial metabolic interference and autophagy-promoted adaptive immunity. *Adv Funct Mater*. 2024;34(8):2310509. doi:10.1002/adfm.202310509
20. Nie Y, Li D, Peng Y, et al. Metal organic framework coated MnO2 nanosheets delivering doxorubicin and self-activated DNAzyme for chemo-gene combinatorial treatment of cancer. *Int J Pharm*. 2020;585:119513. doi:10.1016/j.ijpharm.2020.119513
21. Zheng M, Zhang H, Dai M, et al. A PTT-induced feed-back carbon nanosystem for enhanced breast cancer therapy by extracellular matrix remodeling. *Nano Lett*. 2025;25(8):3180–3190. doi:10.1021/acs.nanolett.4c05625
22. Zhang L, Yang A, Ruan C, et al. Copper-nitrogen-coordinated carbon dots: transformable phototheranostics from precise PTT/PDT to post-treatment imaging-guided PDT for residual tumor cells. *ACS Appl Mater Interfaces*. 2023;15(2):3253–3265. doi:10.1021/acsami.2c17525
23. Zhang W, Yu L, Jiang Y, Guo C. Phycocyanin-functionalized black phosphorus quantum dots enhance PDT/PTT therapy by inducing ROS and irreparable DNA damage. *Biomater Sci*. 2021;9(15):5302–5318. doi:10.1039/D1BM00106J
24. Qin D, Liu C, Song K, Ramakrishna S. Bioinspired silk fibroin/poly-acrylic acid high-performance hydrogel sensors with micro-architecture prepared by rapid polymerization via TA-Fe3O4@MXene catalytic system. *Chem Eng J*. 2025;525:170300. doi:10.1016/j.cej.2025.170300
25. Zhu K, Qian S, Guo H, et al. pH-activatable organic nanoparticles for efficient low-temperature photothermal therapy of ocular bacterial infection. *ACS Nano*. 2022;16(7):11136–11151. doi:10.1021/acsnano.2c03971
26. Chang M, Hou Z, Wang M, et al. Single-Atom Pd nanozyme for ferroptosis-boosted mild-temperature photothermal therapy. *Angew Chem Int Ed*. 2021;60(23):12971–12979. doi:10.1002/anie.202101924
27. Qi M-H, Wang -D-D, Qian W, et al. High-efficiency gold nanoaggregates for NIR LED-driven sustained mild photothermal therapy achieving complete tumor eradication and immune enhancement. *Adv Mater*. 2025;37(5):2412191. doi:10.1002/adma.202412191
28. Yao M, Liang S, Zeng Y, et al. Dual factor-loaded artificial periosteum accelerates bone regeneration. *ACS Biomater Sci Eng*. 2024;10 (4):2200–2211. doi:10.1021/acsbiomaterials.3c01587
29. Masters EA, Ricciardi BF, Bentley KLDM, Moriarty TF, Schwarz EM, Muthukrishnan G. Skeletal infections: microbial pathogenesis, immunity and clinical management. *Nat Rev Microbiol*. 2022;20(7):385–400. doi:10.1038/s41579-022-00686-0
30. Hao X, Jiang B, Wu J, et al. Nanomaterials for bone metastasis. *J Control Release*. 2024;373:640–651. doi:10.1016/j.jconrel.2024.07.067
31. Nadi A, Khodaei M, Javdani M, et al. Fabrication of functional and nano-biocomposite scaffolds using strontium-doped bredigite nanoparticles/ polycaprolactone/poly lactic acid via 3D printing for bone regeneration. *Int J Biol Macromol*. 2022;219:1319–1336. doi:10.1016/j.ijbiomac.2022.08.136
32. Ren S, Zhou Y, Zheng K, et al. Cerium oxide nanoparticles loaded nanofibrous membranes promote bone regeneration for periodontal tissue engineering. *Bioact Mater*. 2022;7:242–253. doi:10.1016/j.bioactmat.2021.05.037
33. Su J, Yang Q, Zhang N, et al. Synergistic effects of thermally induced gradient wettability and pore structure in thermoresponsive polymer-functionalized polyester knitted fabrics for adaptive thermal and moisture regulation. *ACS Appl Mater Interfaces*. 2025;17 (47):64992–65005. doi:10.1021/acsami.5c15482
34. Cheng S, Yang J, Song J, et al. A motion-responsive injectable lubricative hydrogel for efficient Achilles tendon adhesion prevention. *Mater Today Bio*. 2025;30:101458. doi:10.1016/j.mtbio.2025.101458
35. Li L, Lin Y, Liu K, et al. Multiple-effect combined hydrogels: "temporal regulation" treatment of osteosarcoma-associated bone defects with switchable hyperthermia and bioactive agents. *Adv Funct Mater*. 2024;13(31):2402505. doi:10.1002/adhm.202402505
36. Blumberg N, Heal JM. Transfusion-induced immunomodulation and its possible role in cancer recurrence and perioperative bacterial infection. (0044-0086 (Print)).
37. Chu B, Wu S, Yang Y, Song B, Wang H, He Y. Multifunctional flavonoid-silica nanohydrogel enables simultaneous inhibition of tumor recurrence and bacterial infection in post-surgical treatment. *Small*. 2022;18(5):2104578. doi:10.1002/smll.202104578
38. Bohle B, Pera M, Pascual M, et al. Postoperative intra-abdominal infection increases angiogenesis and tumor recurrence after surgical excision of colon cancer in mice. *Surgery*. 2010;147(1):120–126. doi:10.1016/j.surg.2009.06.035
39. Feng Y, Chen J, Ning C. Advances in biomedical applications of Se-based nanozymes. *J Nanobiotechnol*. 2025;23(1):711. doi:10.1186/s12951-025-03770-8